 CMC, vol.39, no.3, pp.267-288, 2014

# Some Applications of Metamaterial Resonators Based on Symmetry Properties

**J. Naqui**[1] **and F. Martín**[1]

**Abstract:** Metamaterial resonators are electrically small resonant particles useful for the implementation of effective media metamaterials. In this paper, some applications of metamaterial resonators (such as the split ring resonator -SRR-, the complementary split ring resonator -CSRR-, the folded stepped impedance resonator -SIR-, and the electric LC resonator), that exploit the symmetry properties of transmission lines loaded with such symmetric particles, are reviewed. This covers differential (balanced) lines with common mode suppression, linear and angular displacement sensors (including alignment sensors), angular velocity sensors, and radiofrequency barcodes. Advantages and drawbacks as compared to existing implementations are also discussed.

**Keywords:** Metamaterials, split ring resonators (SRRs), duality, stepped impedance resonators (SIRs), differential lines, microwave sensors, RF barcodes.

## 1 Introduction

Effective media metamaterials are artificial structures with controllable electromagnetic properties [Marqués, Martín and Sorolla (2008)]. Such media are implemented by means of periodic electrically small inclusions, and their properties depend on how they are structured (or engineered), rather than on the properties of the constitutive materials (typically combinations of dielectrics and metals). Effective media metamaterials are effectively homogeneous structures as long as the guided wavelength is much larger than the relevant dimension (period) of the structure, and such materials are said to exhibit effective (average) media properties. A clear example of a bulk effective media metamaterial is the one reported by Smith and co-workers in 2000 [Smith, Padilla, Vier, Nemat-Nasser and Schultz (2000)], consisting of a combination of split ring resonators (SRRs, see Fig. 1a) [Pendry, Holden, Robbins and Stewart (1999)] and metallic posts. Such artificial structure was the first

[1] GEMMA/CIMITEC, Departament d'Enginyeria Electrònica, Universitat Autònoma de Barcelona, 08193 Bellaterra (Barcelona), Spain.

reported one supporting backward (or left-handed) wave propagation, specifically in a narrow frequency band above the fundamental resonance of the SRRs. This is achieved because the SRRs exhibit a strong diamagnetism in that region, and thus an array of SRRs exhibits a resonant-type negative effective permeability in a certain band above resonance (for incident waves polarized with the magnetic field axial to the rings). Conversely, the metallic posts behave as an effective medium with negative permittivity up to a frequency (plasma frequency) that depends on the distance between posts and their radius (the electric field being parallel to the posts axis) [Pendry, Holden, Robbins and Stewart (1998)]. By properly combining the posts and the SRRs, an effective medium with simultaneous negative permittivity and permeability in a narrow band of the microwave spectrum (for a certain polarization) arises, and the resulting artificial medium supports backward waves in that region. Notice, however, that metals (the constitutive materials of the posts) behave as plasmas (exhibiting negative permittivity) only at optical frequencies. Moreover, neither metals (e.g. copper, aluminum, or gold) nor dielectrics (SRRs are typically made by such cited metals etched on a dielectric slab) exhibit magnetic activity at microwave frequencies. Hence, it is clear that through a proper architecture, it is possible to implement metamaterials with controllable and even unconventional properties, sometimes not found in natural materials (indeed, media exhibiting simultaneous negative permittivity and permeability, also called left-handed media, backward wave media, negative refractive index media, or Veselago media, have not been found in nature to date).

A diamagnetic behavior can also be achieved by folded stepped impedance resonators (SIRs, see Fig. 1b) [Makimoto and Yamashita (1979)]. Such resonant elements are engineered to be electrically small by folding them and by widening their open-ended strip sections (this enhances the resonator capacitance). Thus, folded SIRs are also useful for the implementation of negative effective permeability media.

In 2004, Falcone et al. proposed a novel resonant particle, the complementary counterpart of the SRR (CSRR, see Fig. 1c) useful for the implementation of negative effective permittivity media [Falcone, Lopetegi, Baena, Marqués, Martín and Sorolla (2004)]. This particle is the negative image of the SRR, and, excited by means of an axial electric field, it exhibits a negative effective permittivity in the vicinity of the fundamental CSRR resonance. Indeed, one-dimensional negative permittivity structures can be implemented by loading a microstrip line with an array of CSRRs etched in the ground plane, beneath the conductor strip (similarly, a coplanar waveguide –CPW–with pairs of SRRs etched in the back substrate side exhibits a negative effective permeability [Martín, Falcone, Bonache, Marqués and Sorolla (2003)]).

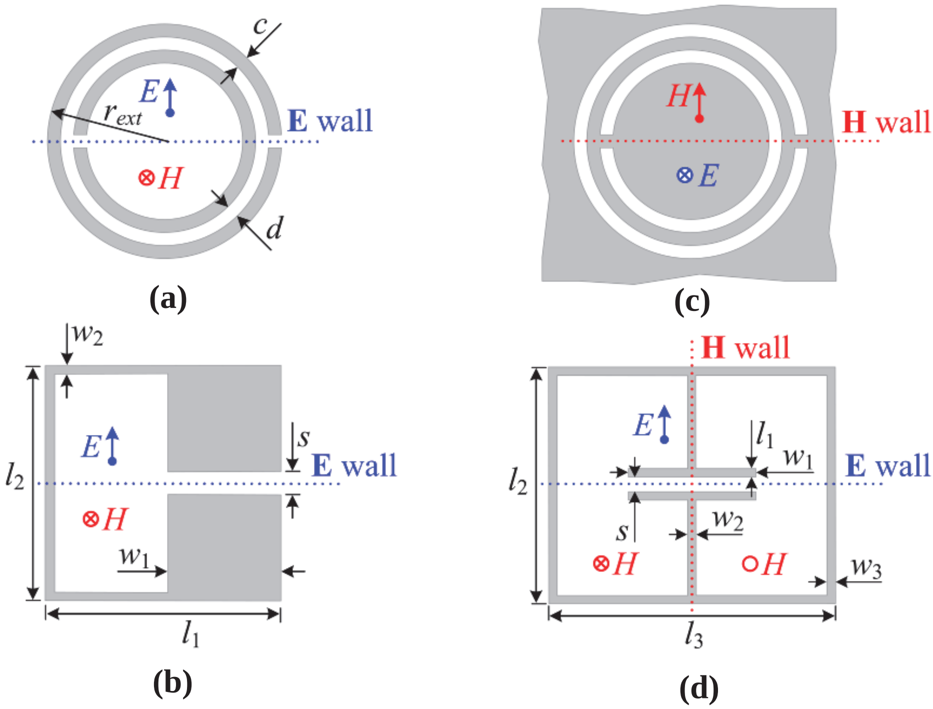


Figure 1: Typical topology of an SRR (a), a folded SIR (b), a CSRR (c), and an ELC resonator (d). The driving mechanisms (electric field or magnetic field excitation), the symmetry planes and the electromagnetic nature of them (electric wall, E wall, or magnetic wall, H wall) at the fundamental resonance are indicated. Notice that the SRR, folded SIR and CSRR can be excited by either a uniform electric field or uniform magnetic field properly oriented (or both simultaneously, phenomenon known as cross-polarization). For the ELC, an axial uniform magnetic field is not able to drive the particle, but it can be excited by counter magnetic fields applied at both halves of the particle, as illustrated

The last metamaterial particle of interest for the purposes of this paper is the so-called electric LC (ELC) resonator (Fig. 1d), first proposed by [Schurig, Mock and Smith (2006)]. This particle is made by means of two open loops in contact by the gap region. This particle cannot be excited at its fundamental resonance by means of a uniform magnetic field since the currents have opposite directions in both rings at such resonance. However, the ELC can be excited by means of a uniform electric field applied in the direction orthogonal to the symmetry plane along the gap (notice that this particle has two orthogonal symmetry planes). Consequently, this particle can be used for the implementation of resonant-type negative effective permittivity media.

In the present work, the above-cited metamaterial resonators are combined with transmission lines for the implementation of various types of microwave devices, where their functionality is based on symmetry properties. Hence, our aim is not to implement effective media metamaterials or transmission line metamaterials (one-dimensional metamaterials implemented by loading a host transmission line) and devices based on them, but to exploit the symmetry of these metamaterial resonators and the properties derived from that symmetry, for the design of functional microwave devices, including common-mode suppression filters for balanced lines, microwave sensors, and RF barcodes.

## 2 On the symmetry properties of transmission lines loaded with symmetric metamaterial resonators

Typically, when a transmission line is loaded with a resonator coupled to it, the transmission coefficient exhibits a notch at the fundamental resonance frequency (and at higher-order resonances as well), and the injected power is reflected back to the source. This has been verified, for instance, in CPW transmission lines loaded with pairs of SRRs [Martín, Falcone, Bonache, Marqués and Sorolla (2003); Falcone, Martín, Bonache, Marqués and Sorolla (2004)] and in microstrip lines loaded with CSRRs [Falcone, Lopetegi, Baena, Marqués, Martín and Sorolla (2004)]. However, depending on the relative orientation between the line and the resonators, it is possible to prevent the appearance of the notch in the transmission coefficient at a particular resonance frequency. To clarify this, let us consider a CPW transmission line loaded with a single SRR (Fig. 2) [Naqui, Durán-Sindreu and Martín (2011)]. For the specific SRR orientation of Fig. 2(a), i.e., with perfect alignment between the symmetry planes of the line and resonator, the particle can neither be excited by the magnetic field nor by the electric field generated by the line. For such orientation, the axial magnetic field components within the SRR perfectly cancel, and the particle cannot be magnetically driven. Similarly, the particle cannot be excited by the line electric field since the transversal electric field components in the plane of the particle do also cancel. However, if the particle is either rotated or transversally shifted, this perfect cancellation of field components vanishes, currents are induced in the SRR, and a notch in the transmission coefficient appears. The key aspect to prevent particle excitation is a perfect alignment between the symmetry plane of the line (magnetic wall in a CPW) and the symmetry plane of the particle (electric wall for the SRR at the fundamental resonance). Thus, if the symmetry planes of the line and resonator are perfectly aligned and they are of distinct electromagnetic nature (one being a magnetic wall and the other an electric wall), the resonator is not excited. If this condition is not fulfilled, either because the line and resonator are not aligned or because they are aligned but both symmetry planes are of the same nature (either magnetic walls or electric walls), then the resonator is excited and the line exhibits a transmission zero (notch). This property holds for other transmission lines and symmetric resonators (as those depicted in Fig. 1) as well, and it can be of interest for the implementation of functional microwave devices, as will be demonstrated in the next sections.

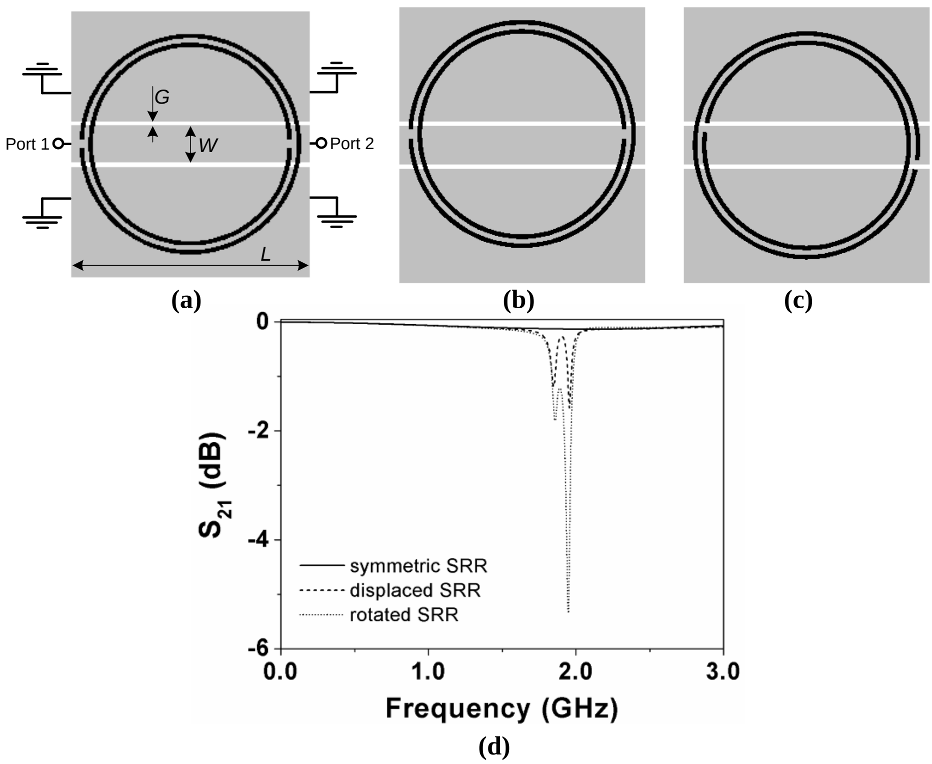


Figure 2: CPW transmission line loaded with a circular SRR perfectly aligned with the line (a), laterally shifted (b) and rotated (c), and the corresponding frequency responses (d) (simulated by means of the Agilent Momentum commercial EM software). The considered substrate is Rogers RO3010 with dielectric constant $\varepsilon_r$ = 10.2 and thickness $h$ = 127 $\mu$m. Dimensions are: $L$ = 10.4 mm, $W$ = 1.67 mm, $G$ = 0.2 mm, $c$ = $d$ = 0.2 mm, $r_{ext}$ = 5 mm. Figure extracted from [Naqui, Durán-Sindreu, and Martín (2011)], reprinted with permission

## 3 Common-mode suppression filters for balanced lines

Differential (or balanced) transmission lines exhibit high immunity to noise, electromagnetic interference, and crosstalk. These lines are of interest in high-speed digital circuits based on differential signals, and, in general, in applications where circuits are subjected to noisy environments. In balanced lines with a common ground plane, the suppression of the common mode in the region of interest, while keeping the integrity of the differential signals unaltered is a due. There are several approaches for the suppression of the common mode in differential lines. The common-mode filters based on low temperature co-fired ceramic (LTCC) technology reported in [Tseng and Wu (2004)], or the negative permeability structures of [Tsai and Wu (2010)], are compact and provide efficient common-mode rejection over wide frequency bands, but they are technologically complex. Common-mode filters based on defected ground structures were also reported. In [Liu, Tsai, Han and Wu (2008)], dumbbell shaped periodic patterns etched in the ground plane, underneath the differential lines, were used to suppress the common mode (even mode) by opening the return current path through the ground plane. This has small effect on the differential signals (odd mode) since relatively small current density returns through the ground plane for such signals. In [Wu, Tsai, Wu and Itoh (2009)], a wide stop-band for the common mode was achieved by using U-shaped and H-shaped coupled resonators, symmetrically etched in the ground plane.

Alternatively, the common mode can be efficiently suppressed by loading a microstrip balanced line with an array of CSRRs with its symmetry plane (a magnetic wall at the fundamental resonance) aligned with the symmetry plane of the line (Fig. 3a) [Naqui, Fernández-Prieto, Durán-Sindreu, Selga, Medina, Mesa and Martín (2011); Naqui, Fernández-Prieto, Durán-Sindreu, Mesa, Martel, Medina and Martín (2012)]. For the common mode, the symmetry plane of the line is a magnetic wall. Therefore, since the CSRR symmetry plane is also a magnetic wall, a notch in the transmission coefficient for the common mode is expected for a line loaded with a CSRR. Conversely, for the differential mode the symmetry plane of the line is an electric wall, and, according to the previous section, the line should be transparent for that mode. To gain insight on this, the lumped-element equivalent circuit model of a CSRR-loaded differential line without considering losses is depicted in Fig. 3(b). Coupling between adjacent resonators is not accounted for in this model, but it was considered in [Naqui, Fernández-Prieto, Durán-Sindreu, Mesa, Martel, Medina and Martín (2012)], where it was demonstrated that such coupling enhances the common-mode suppressed band as a result of the presence of complex modes (i.e., modes that usually appear as conjugate pairs and do not carry a net power). The inductance of the line is modeled by $L$, the electric coupling between the line and the resonator is accounted for by $C$, the CSRR is modeled by the parallel resonant tank, $L_c - C_c$, and, finally, $C_m$ and $L_m$ model the mutual capacitance and inductance between the coupled lines, respectively. Note that the dominant line-to-resonator coupling is electric, and for this reason the magnetic coupling is neglected for the sake of simplicity. For the differential mode, the resonator is short circuited to ground, and the resulting model (Fig. 4a) is the one of a conventional transmission line. Contrarily, for the common mode, we obtain the same circuit as that of a CSRR-loaded line [Baena, Bonache, Martín, Marqués, Falcone, Lopetegi, Laso, García, Gil, Flores-Portillo and Sorolla (2005)], but with modified parameters (Fig. 4b). Thus, we do expect a similar stop-band behavior for the common mode.

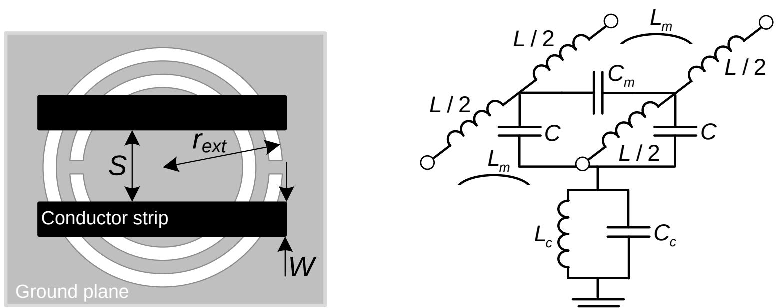


**(a)** **(b)**

Figure 3: Topology (a) and circuit model (b) of a differential microstrip line loaded with a CSRR.

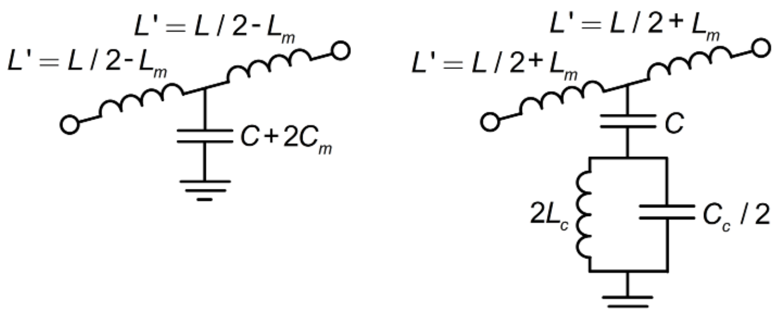


**(a)** **(b)**

Figure 4: Circuit models of a CSRR-loaded differential microstrip line for the differential mode (a) and common mode (b).

To validate the model for the common mode, Fig. 5 compares the electromagnetic and circuit simulation of the structure depicted in the inset. The circuit parameters of the model were extracted according to the procedure reported in [Bonache, Gil, Gil, Garcia-García and Martín (2006)]. There is good agreement between the circuit and electromagnetic simulation. Hence, the model is validated.

Typically, to broaden the common-mode suppression band, square or rectangular shaped CSRRs are used since the coupling between adjacent resonators is enhanced. However, it is also important that the individual resonators provide as much rejection bandwidth as possible, and, to this end, it is necessary to increase the coupling capacitance, $C$, and to reduce the inductance, $L_c$, and capacitance, $C_c$, of the CSRR [Naqui, Fernández-Prieto, Durán-Sindreu, Selga, Medina, Mesa and Martín (2011); Naqui, Fernández-Prieto, Durán-Sindreu, Mesa, Martel, Medina and Martín (2012)]. According to it, weakly coupled lines are convenient, since the width of the lines necessary to achieve an odd mode impedance of 50Ω is wider, and this enhances the coupling capacitance of the even mode. To reduce the inductance and capacitance of the CSRR, maintaining the coupling level, it is necessary to increase the rings width, $c$, and separation, $d$. This results in a larger CSRR size (for a given transmission zero frequency), but the achievable bandwidth is also larger. Obviously, under these conditions the validity of the circuit model is limited to a much smaller frequency band, but the interest in common-mode suppression filters is to enhance the common-mode rejection band as much as possible. A systematic approach for the design of common-mode filters is reported in [Naqui, Fernández-Prieto, Durán-Sindreu, Mesa, Martel, Medina and Martín (2012)]. To illustrate the possibilities of the CSRRs to suppress the common mode in differential lines, Fig. 6 depicts a fabricated prototype, and the frequency response. The dimensions of the active region of the structure are 32.8 mm × 10.8 mm, that is $0.43\lambda_e \times 0.14\lambda_e$, where $\lambda_e$ is the even-mode guided wavelength at the central frequency. The measured insertion loss for the differential signal is smaller than 0.5 dB in the considered range, being the loss tangent of the substrate $\tan\delta = 0.0023$. The structure of Fig. 6 is compared with other ones reported in the references (see Tab. 1). The combination of size, bandwidth and stop-band rejection is competitive. The structure in [Tsai and Wu (2010)] exhibits small dimensions and relatively wide bandwidth, but it needs three metal levels. In summary, the CSRR-based approach is a promising alternative for the design of differential lines with common-mode suppression. Notice that although the theory of effective media metamaterials has not been invoked, the structure of Fig. 6 can be considered a 3-cell one-dimensional negative effective permittivity medium for the common mode.

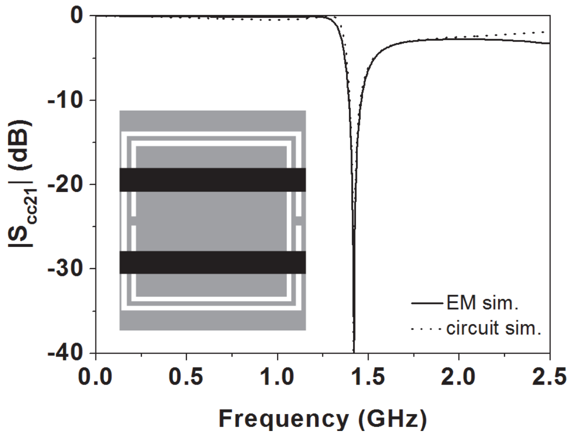


Figure 5: Simulated common-mode insertion loss $|S_{cc21}|$ for the structure shown in the inset. CSRR dimensions are: $c$ = 0.2 mm, $d$ = 0.2 mm, $W$ = 1 mm, $S$ = 2.5 mm, and side length 7.6 mm. Extracted parameters are $L'$ = 4.93 nH, $C$ = 1.06 pF, $C_c$ = 2.68 pF and $L_c$ = 3.36 nH. The considered substrate is *Rogers RO3010* with dielectric constant $\varepsilon_r$ = 10.2 and thickness $h$ = 1.27 mm. Figure extracted from [Naqui, Fernández-Prieto, Durán-Sindreu, Selga, Medina, Mesa and Martín (2011)], reprinted with permission.

## 4 Microwave sensors

Microwave sensors are usually based on the change of resonance frequency, phase or quality factor of a microwave resonator, caused by the physical variable to be sensed. A recent reported approach for the implementation of microwave sensors relies on the basis of symmetry perturbation in transmission lines loaded with symmetric metamaterial resonators. Therefore, sensors based on symmetry properties can be implemented, in which, typically, the depth of the notch (transmission zero) depends on the level of asymmetry caused by the changing physical variable. As compared to sensors based on the variation of the resonance frequency, the sensors based on symmetry properties by inspection of the notch depth are more robust in front of changing environmental conditions, though they are more sensitive to noise.

The symmetry in transmission lines loaded with metamaterial resonators can be perturbed by several mechanisms, such as by a relative displacement (linear or angular) between the transmission line and the resonator, or by means of an asymmetric dielectric loading. Thus, the proposed sensing principle is useful for the design of novel linear displacement sensors [Horestani, Fumeaux, Al-Sarawi and Abbott

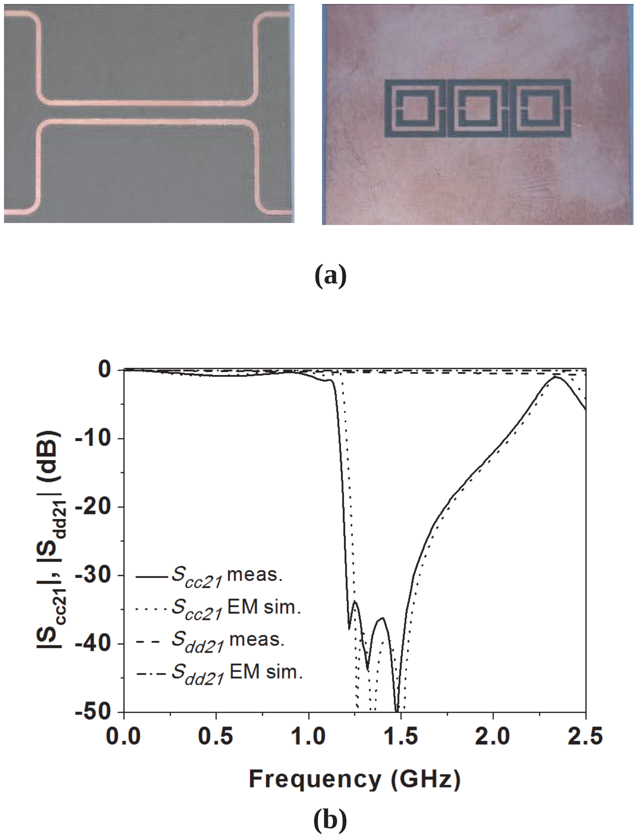


Figure 6: Photograph of a differential line with wideband common-mode rejection (a), and common-mode and differential-mode insertion loss (b). Losses in the electromagnetic simulation are considered. The differential line is loaded with three square-shaped CSRRs separated 0.2 mm, with $c$ = 1.2 mm, $d$ = 0.8mm, and a side length of 10.8 mm. Figure extracted from [Naqui, Fernández-Prieto, Durán-Sindreu, Selga, Medina, Mesa, and Martín (2011)], reprinted with permission.

(2013); Horestani, Naqui, Shaterian, Abbott, Fumeaux and Martín (2014); Naqui, Durán-Sindreu and Martín (2011); Naqui, Durán-Sindreu and Martín (2012a)], angular displacement sensors [Horestani, Abbott and Fumeaux (2013); Naqui, Durán-Sindreu and Martín (2011); Naqui, Durán-Sindreu, and Martín (2013b); Naqui and Martín (2013)], rotation speed sensors [Naqui and Martín (2013); Naqui and Martín (2014)], sensors for dielectric characterization [Naqui, Damm, Wiens, Jakoby, Su and Martín (2014)], among others. To illustrate the potential of this novel sensing

Table 1: Comparison of several differential lines with common-mode suppression. FBW is the fractional stopband bandwidth.

| *Ref.* | *Length* ($\lambda_e$) | *Width* ($\lambda_e$) | *Area* ($\lambda_e^2$) | *FBW* (%) | | |
|---|---|---|---|---|---|---|
| | | | | $-10$ dB | $-20$ dB | $-40$ dB |
| [Liu, Tsai, Han, and Wu (2008)] | 0.76 | 0.47 | 0.36 | 70 | 53 | - |
| [Wu, Tsai, Wu, and Itoh (2009)] | 0.44 | 0.44 | 0.19 | 87 | - | - |
| [Tsai and Wu (2010)] | 0.26 | 0.16 | 0.04 | 60 | 32 | - |
| [Naqui, Fernández-Prieto, Durán-Sindreu, Selga, Medina, Mesa, and Martín (2011)] | 0.43 | 0.14 | 0.06 | 54 | 37 | 14 |
| [Naqui, Fernández-Prieto, Durán-Sindreu, Mesa, Martel, Medina, and Martín (2012)] | 0.64 | 0.13 | 0.08 | 51 | 41 | 23 |

approach, an angular displacement and rotation speed sensor, reported in [Naqui and Martín (2013)], is considered here. The sensor simply consists of a circular-shaped CPW transmission line loaded with an ELC resonator, also circular. By choosing a circular shape for both the line and the resonator the linearity (i.e., the deviation from a straight line in the dependence of the notch depth with the rotation angle) is improved. A typical topology is illustrated in Fig. 7.

The lumped element equivalent circuit model of the structure of Fig. 7 is depicted in Fig. 8(a). This circuit is valid as long as the cell length is electrically small and losses are not considered. The ELC resonator is represented by the inductances $L_e$ and the capacitance $C_e$, modeling the inductive loops and the capacitive gap, respectively. The CPW is modeled by its inductance and capacitance, $L$ and $C$, respectively, and it is divided into two identical halves for convenience. Finally, each half is magnetically coupled to each loop through the mutual inductances $M_\theta$ and $M^\theta$, both being dependent on the angle $\theta$ (different dots are used to distinguish the magnetic coupling sign associated to each of the halves). Therefore, the frequency response of the circuit of Fig. 8(a) directly depends on $\theta$. When there is alignment between walls of different nature, $\theta = 0^{\circ}$, due to symmetry, $M_\theta = M^\theta \neq 0$, which means that the currents flowing on the CPW induce a pair of equal and anti-phase voltages in the loops; no net voltage is induced in the resonator due to an absolute cancellation. In other words, there is not a net magnetic coupling, the resonator

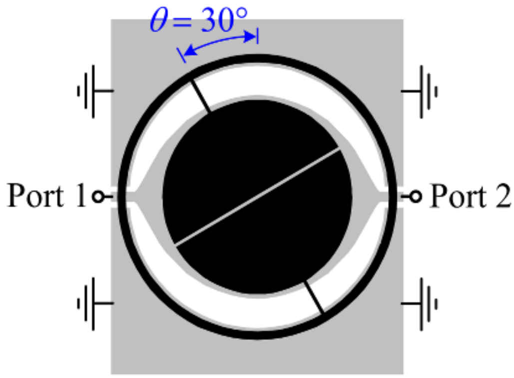


Figure 7: Layout of a circular-shaped CPW loaded with a circular ELC (for a specific angle of $\theta = 30^{\circ}$). The considered substrate is *Rogers RO3010* with $h = 1.27$ mm and $\varepsilon_r = 11.2$. The dimensions are: for the line, $W$ and $G$ are tapered such that the characteristic impedance is 50 Ω; for the ELC resonator: mean radius $r_0 = 8.05$ mm, capacitor outer radius $r_1 = 11$ mm, $w_2 = s = 0.2$ mm, and $w_3 = 0.5$ mm.

cannot be magnetically driven, and the resulting model is that of a conventional transmission line. On the other hand, as $\theta$ increases the magnetic coupling is complementarily distributed; $M^{\theta}$ increases at the expense of a decrease in $M_{\theta}$. Hence for $\theta > 0^{\circ}$, a net induced voltage arises and the line is indeed capable of magnetically excite the resonator. The larger the angle, the higher the induced voltage. Thus at the upper limit, when walls of the same electromagnetic nature are aligned, $\theta = 90^{\circ}$, $M^{\theta}$ is maximum while $M_{\theta}$ completely vanishes; the magnetic coupling cancellation disappears and the resonator is expected to be tightly coupled to the line. The physical understanding of magnetic coupling cancellation relative to the resonator orientation is well illustrated by this model. Nevertheless, such circuit is somewhat complex and has too many parameters for both parameter extraction and design purposes. An equivalent and simplified circuit model is the one depicted in Fig. 8(b), where an effective mutual inductance $M$ is defined. Such model is equivalent to that of an SRR magnetically coupled to a CPW transmission line, which can be transformed to the circuit model of Fig. 8(c) [Aznar, Gil, Bonache, Jelinek, Baena, Marqués and Martín (2008)]. From the latter model, it can be concluded that there is not only a transmission zero at $f_0$ as long as $M$ is different than zero, but also the rejection bandwidth broadens with $M$ (the reason is that the susceptance slope of the parallel resonator decreases as the ratio $L'_e/C'_e$ increases). Furthermore, the lumped element values of that circuit can be easily extracted from the method reported in [Aznar, Gil, Bonache, Jelinek, Baena, Marqués and Martín (2008)].

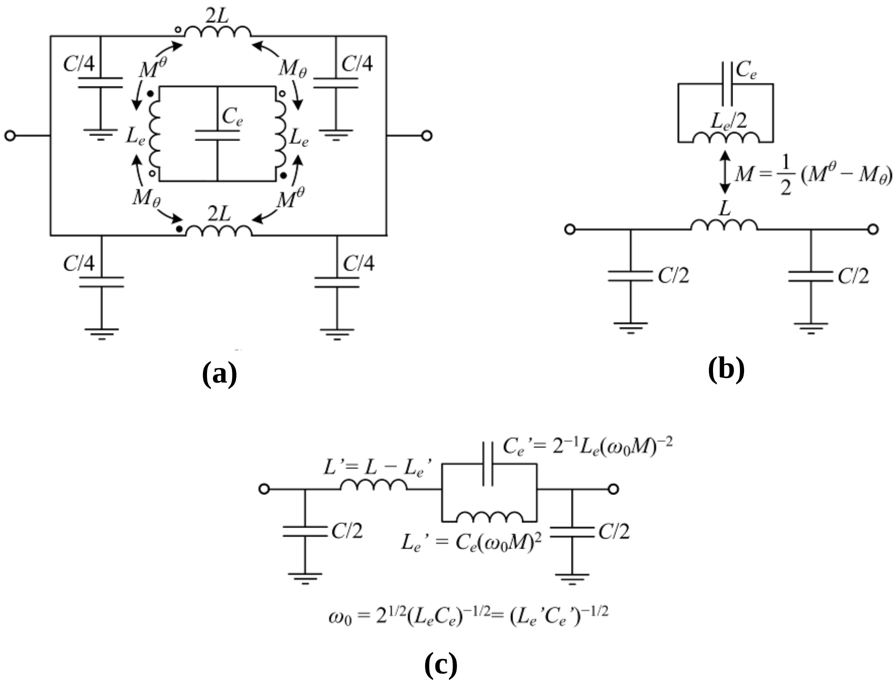


Figure 8: (a) Equivalent circuit model of a CPW loaded with an ELC resonator as the one shown in Fig. 7, including the different magnetic coupling mechanisms, accounted for through the mutual inductances $M_{\theta}$ and $M^{\theta}$; (b) simplified circuit model; (c) transformed simplified circuit model.

Fig. 9 depicts the frequency response of the structure of Fig. 7 for different rotation angles. The parameters of the circuit of Fig. 8(b) have been extracted, and it is remarkable that with the exception of the mutual inductance, all the circuit parameters are roughly invariant with the rotation angle (see Tab. 2). The responses of the circuit of Fig. 8(b) inferred from the extracted parameters are also included in Fig. 9. The agreement between the circuit and electromagnetic simulations is good. Thus, the proposed model is validated. Interestingly, $M$ varies roughly linearly with the rotation angle, and it was demonstrated in [Naqui and Martín (2013)] that the notch depth in dB (considering losses) is also nearly linear. This is interesting for the use of these structures as rotation sensors.

In the structure of Fig. 7, the ELC is etched on the back substrate side of the CPW. This structure (with different rotation angles of the ELC) was solely implemented for validation of the equivalent circuit model. In a practical rotation sensor, the ELC must be etched on another (movable) substrate, with an air gap between the

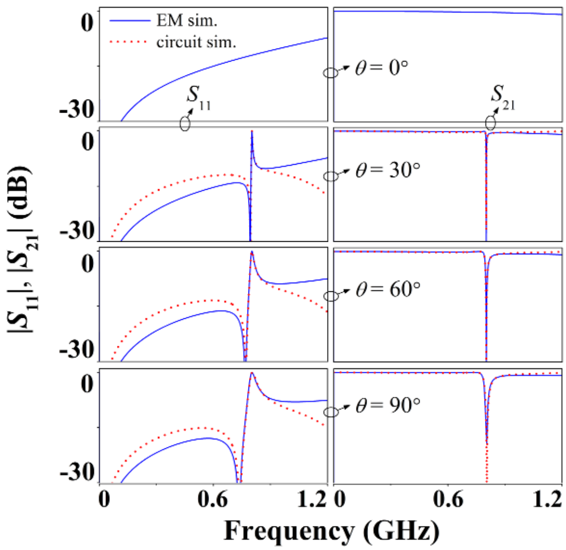


(a)

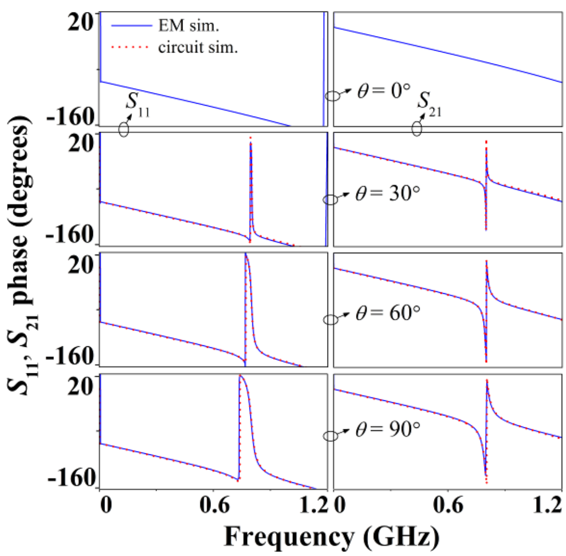


(b)

Figure 9: (a) Magnitude and (b) phase of the reflection and transmission coefficients given by the electromagnetic simulation for the structure of Fig. 7 and by the circuit simulation for the models of Fig. 8. The circuit parameters are those given in Tab. 2.

Table 2: Extracted lumped element values of the circuit of Fig. 8(b) for the structure of Fig. 7.

| $\theta$ (degrees) | $C$ (pF) | $L$ (nH) | $C_e$(pF) | $L_e$ (nH) | $M$ (nH) |
|---|---|---|---|---|---|
| 30 | 5.86 | 5.95 | 3.09 | 25.6 | 0.94 |
| 60 | 5.73 | 6.22 | 3.09 | 25.6 | 1.91 |
| 90 | 5.59 | 6.40 | 3.07 | 25.6 | 2.72 |

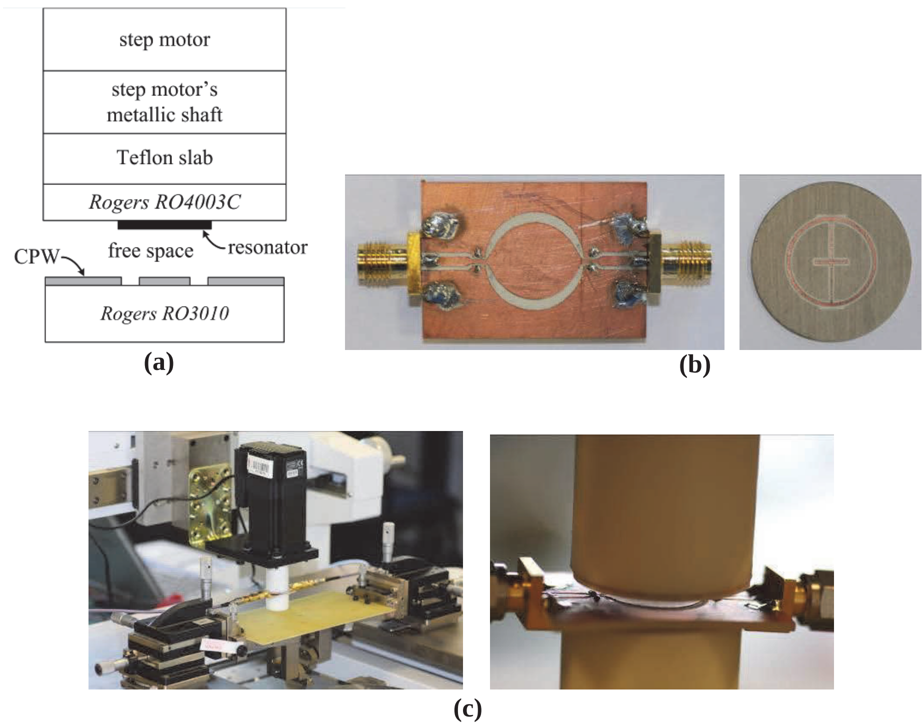


Figure 10: Set-up for the angular displacement measurement; (a) layer cross-section, (b) photograph of the fabricated CPW and ELC resonator, and (c) photographs of the experimental set-up with positioners and a step motor *STM 23Q-3AN*. The ELC-loaded CPW dimensions are those given in the caption of Fig. 7 with the exception of $l_1 = 0.2$ mm and $w_1 = 6$ mm. The parameters of the substrates are: *Rogers RO3010*, $\varepsilon_r = 11.2$, $h = 1.27$ mm, and $\tan\delta = 0.0023$; *Rogers RO4003C*, $\varepsilon_r = 3.55$, $h = 0.8128$ mm, and $\tan\delta = 0.0021$; Teflon, $\varepsilon_r = 2.08$, $h = 3.5$ mm, and $\tan\delta = 0.0004$; in-between air layer, $h = 1.27$ mm, $\varepsilon_r = 1$, and $\tan\delta = 0$.

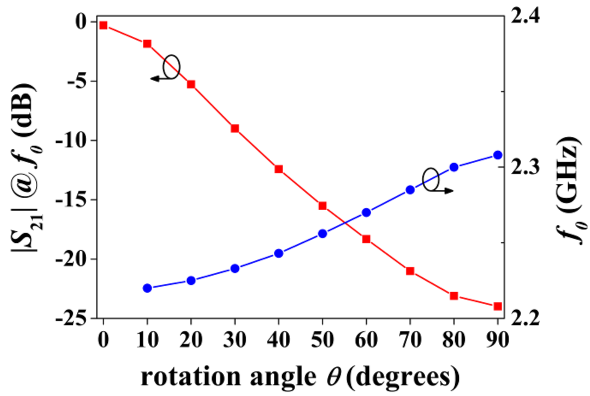


Figure 11: Transfer function of the notch magnitude at the notch frequency in the transmission coefficient versus the rotation angle.

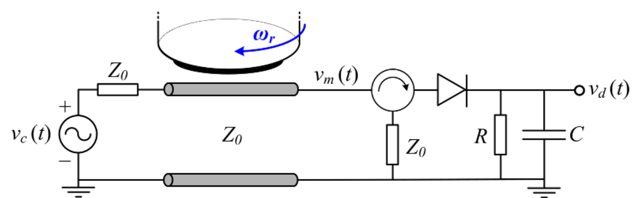


Figure 12: Schematic of the proposed angular velocity sensor.

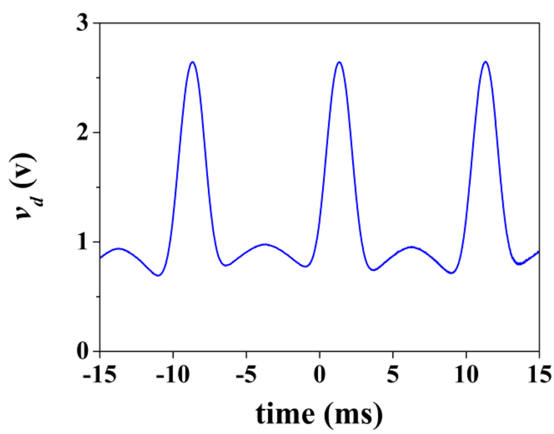


Figure 13: Measured envelope signal for $f_r$ = 50 Hz. Figure extracted from [Naqui and Martín (2013)], reprinted with permission.

substrate supporting the CPW and the one supporting the ELC. A practical rotation sensor is depicted in Fig. 10. The sensor was tested in a realistic experimental set-up, also shown in Fig. 10. The resonator substrate is attached to the metallic shaft of a step motor by means of a Teflon cylindrical slab. The latter is used to avoid close proximity between the resonator and the metallic shaft. Otherwise, the electrical performance of the sensor may change. Given that a step motor divides a full rotation into discrete and equal steps, the angular position can be accurately controlled by holding the position at one of these steps. The step motor *STM 23Q-3AN*, configured with a step resolution of 36,000 steps/revolution, is used (it can be easily controlled through software from a host computer). After a three-dimensional spatial calibration between the CPW and the resonator by means of positioners, the measured notch magnitude as a function of the rotation is plotted in Fig. 11. It is remarkable a high output dynamic range (23.7 dB) while preserving very low insertion loss for small angles (0.29 dB for 0°). The average sensitivity is 0.26 dB/$^o$ and the response is reasonably linear.

The previous rotation sensor can be used for measuring angular velocities. The schematic is depicted in Fig. 12. The idea is to feed the CPW with a harmonic signal tuned in the vicinity of the notch frequencies (the notch position varies slightly with the rotation angle). The rotation has the effect of modulating the amplitude of the feeding signal at the output of the sensing CPW. Through a circulator (to avoid unwanted reflections) and an envelope detector, the envelope can be inferred and monitored by means of an oscilloscope. The time between two adjacent peaks is half a period; therefore, the angular velocity can easily be obtained. Further details of the experimental set-up are given in [Naqui and Martín (2013)].

Fig. 13 shows the signal obtained with an oscilloscope for a rotation speed of 50 Hz, where the distance between adjacent peaks is 10 ms, as expected. These sensors can be used for measuring unlimited rotation speeds, and their cost can be reduced by substituting the circulator, envelope detector and oscilloscope by a digital post processing stage. Accuracy can be enhanced by simply measuring the distance between distant peaks.

## 5 RF barcodes

The symmetry properties of transmission lines loaded with metamaterial resonators can also be applied to the implementation of RF barcodes. These chipless RFID tags can be implemented by loading a transmission line with several resonant elements, each one tuned to a different frequency and corresponding to a different bit. The logic state ‘1’ or ‘0’ given by each resonator is selected by allowing the corresponding resonance frequency to appear, or not, as a notch in the transmission coefficient. It is remarkable the 35-bit RF barcode proposed by the Group of Prof.

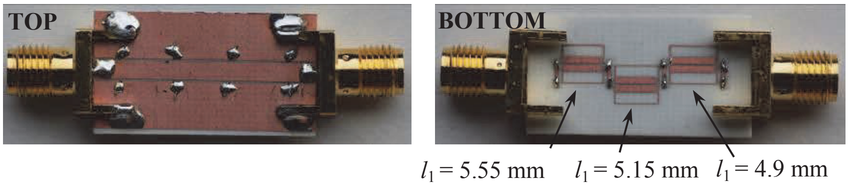


Figure 14: Fabricated CPW loaded with 3 folded SIRs corresponding to the binary code '111' of the designed 3-bit RF barcode. The substrate is *Rogers RO4003C* with $\varepsilon_r = 3.55$, $h = 0.8128$ mm, and $\tan\delta = 0.0021$. CPW dimensions are: $L = 23.9$ mm, $W = 2.16$ mm, and $G = 0.15$ mm; SIR dimensions are: $w_1 = 0.825$ mm, $w_2 = 0.15$ mm, $s = 0.15$ mm, $l_2 = 4.47$ mm, and $l_1$ is shown in the photograph.

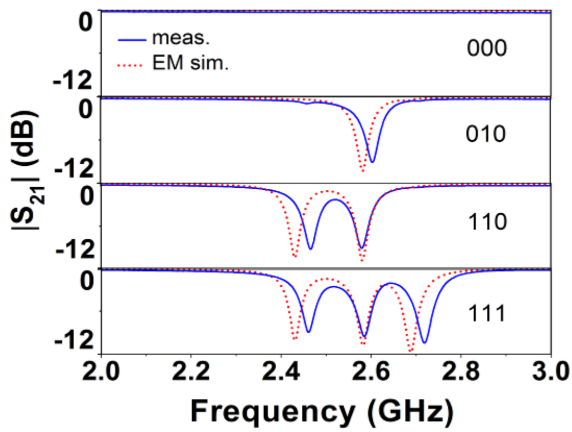


Figure 15: Simulated and measured transmission coefficient of the structure of Fig. 14 and those corresponding to the indicated codes. Figure extracted from [Naqui, Durán-Sindreu and Martín (2012b)], reprinted with permission.

Karmakar, where a microstrip line was loaded with spiral resonators [Preradovic and Chandra-Karmakar (2010)]. The strategy to switch from the '1' state (notch) to the '0' state is to short-circuit the spiral resonator (the resonance frequency changes dramatically), or simply to eliminate it. An alternative to that approach is to load a transmission line with symmetric resonators exhibiting a symmetry plane of different electromagnetic nature than that of the symmetry plane of the line. The '0' state is achieved by merely aligning the resonator and the line, whereas the '1' state is set, for instance, by laterally displacing it. This approach has two advantages: it eases (i) to implement mechanically reconfigurable barcodes, and (ii) to associate more than two logic states to a single resonant element (this is due to the fact that the notch depth depends on the displacement level, and it can be used to encode with multiple thresholds). To illustrate the potential of the approach, we report here a simple (preliminary) structure consisting of a CPW loaded with folded SIRs (Fig. 14) [Naqui, Durán-Sindreu, and Martín (2012b)]. The structure is a 3-bit barcode with the binary code '111'. The frequency response of this structure is depicted in Fig. 15, where other binary codes are also depicted. Folded SIRs can be also used for the implementation of RF barcodes in microstrip technology [Naqui, Durán-Sindreu, and Martín (2013a)].

## 6 Conclusions

In this paper, transmission lines loaded with symmetric metamaterial resonators have been reviewed on the basis of symmetry properties. The principle of operation of such structures relies on the fact that resonance is prevented only for a specific alignment between the symmetry planes of the resonator and the line, corresponding when such planes are of distinct electromagnetic nature (electric and magnetic). In order to validate this statement, equivalent circuit models have been derived and electromagnetic simulations as well as measurements have been performed. Finally, this symmetry-based approach has been shown to be very useful for the implementation of functional devices, such as common-mode suppressed differential lines, microwave sensors, and RF barcodes.

**Acknowledgement:** This work has been supported by MICIIN-Spain (contract TEC2010-17512, CSD2008-00066 and TEC2011-13615-E), and by Generalitat de Catalunya (project 2009SGR-421). Jordi Naqui has been awarded with a FPU Grant by MECD-Spain (Reference AP2010-0431). Ferran Martín is in agreement with Institució Catalana de Recerca i Estudis Avançats (ICREA) for awarding him with an ICREA Academia Award.

## References

**Aznar, F.; Gil, M.; Bonache, J.; Jelinek, L.; Baena, J. D.; Marqués, R; Martín, F.** (2008): Characterization of miniaturized metamaterial resonators coupled to planar transmission lines through parameter extraction. *J. Appl. Phys.*, vol. 104, paper 114501.

**Baena, J. D.,; Bonache, J.; Martín, F.; Marqués, R.; Falcone, F; Lopetegi, L.; Laso, M. A. G.; García, J.; Gil, I; Flores-Portillo, M.; Sorolla, M.** (2005): Equivalent circuit models for split ring resonators and complementary split rings resonators coupled to planar transmission lines. *IEEE Trans. Microw. Theory*

*Techn.*, vol. 53, pp. 1451-1461.

**Bonache, J.; Gil, M.; Gil, I.; Garcia-García, J.; Martín, F.** (2006): On the electrical characteristics of complementary metamaterial resonators. *IEEE Microw. Wirel. Comp. Lett*, vol. 16, pp. 543-545.

**Falcone, F.; Lopetegi, T.; Baena, J. D.; Marqués, R.; Martín, F.; Sorolla, M.** (2004): Effective negative-epsilon stop-band microstrip lines based on complementary split ring resonators. *IEEE Microw. Wireless Comp. Lett.*, vol. 14, pp. 280-282.

**Falcone, F.; Martín, F.; Bonache, J.; Marqués, R.; Sorolla, M.** (2004): Coplanar waveguide structures loaded with split ring resonators. *Microw. Opt. Techn. Let.*, vol. 40, pp. 3-6.

**Horestani, A.; Fumeaux, C.; Al-Sarawi, S.; Abbott, D.** (2013): Displacement sensor based on diamond-shaped tapered split ring resonator. *IEEE Sensors Journal*, vol. 13, no. 4, pp. 1153-1160.

**Horestani, A.; Abbott, D.; Fumeaux, C.** (2013): Rotation sensor based on horn-shaped split ring resonator. *IEEE Sensors Journal*, vol. 13, no. 8, pp. 3014-3015.

**Horestani, A. K.; Naqui, J.; Shaterian, Z.; Abbott, D.; Fumeaux, C.; Martín, F.** (2014): Two-Dimensional Alignment and Displacement Sensor based on Movable Broadside-coupled Split Ring Resonators. *Sensors and Actuators A*. to be published.

**Liu, W. T.; Tsai, C.-H.; Han, T.-W.; Wu, T.-L.** (2008): An embedded common-mode suppression filter for GHz differential signals using periodic defected ground plane. *IEEE Microw. Wireless Comp. Lett.*, vol. 18, no. 4, pp. 248-250.

**Marqués, R.; Martín, F.; Sorolla, M.** (2008): *Metamaterials with Negative Parameters: Theory, Design and Microwave Applications*, John Wiley & Sons, Hoboken.

**Martín, F.; Falcone, F.; Bonache, J.; Marqués, R.; Sorolla, M.** (2003): Split ring resonator based left handed coplanar waveguide. *Appl. Phys. Lett.*, vol. 83, pp. 4652-4654.

**Makimoto, M.; Yamashita, S.** (1979): Compact Bandpass Filters Using Stepped Impedance Resonators. *Proc. IEEE*, vol. 67, pp. 16-19.

**Naqui, J.; Durán-Sindreu, M.; Martín, F.** (2011): Novel Sensors Based on the Symmetry Properties of Split Ring Resonators (SRRs). *Sensors*, vol 11, pp. 7545-7553.

**Naqui, J.; Fernández-Prieto, A.; Durán-Sindreu, M.; Selga, J.; Medina, F.; Mesa, F.; Martín, F.** (2011): Split Rings-Based Differential Transmission Lines with Common-Mode Suppression. *IEEE MTT-S Int. Microwave Symposium*, Baltimore, USA.

**Naqui, J.; Durán-Sindreu, M.; Martín, F.** (2012): Alignment and Position Sensors Based on Split Ring Resonators. *Sensors*, vol. 12, pp. 11790-11797.

**Naqui, J.; Durán-Sindreu, M; and Martín, F.** (2012): On the Symmetry Properties of Coplanar Waveguides Loaded with Symmetric Resonators: Analysis and Potential Applications. *IEEE MTT-S Int. Microwave Symp.*, Montreal, Canada.

**Naqui, J.; Fernández-Prieto, A; Durán-Sindreu, M.; Mesa, F; Martel, J; Medina, F.; Martín, F.** (2012): Common mode suppression in microstrip differential lines by means of complementary split ring resonators: theory and applications. *IEEE Trans. Microw. Theory Techn.*, vol. 60, pp. 3023-3034.

**Naqui, J; Durán-sindreu, M; Martín, F.** (2013): Strategies for the implementation of sensors and RF barcodes based on transmission lines loaded with symmetric resonators. *21st International Conference on Applied Electromagnetics and Communications* (ICECom 2013), Dubrovnik, Croatia.

**Naqui, J.; Durán-Sindreu, M; Martín, F.** (2013): Transmission Lines Loaded with Bisymmetric Resonators and Applications. *IEEE MTT-S Int. Microwave Symp.*, Seattle USA.

**Naqui, J.; Martín, F.** (2013): Transmission Lines Loaded with Bisymmetric Resonators and Their Application to Angular Displacement and Velocity Sensors. *IEEE Trans. Microw. Theory Techn.*, vol. 61(12), pp. 4700-4713.

**Naqui, J; Martín, J.** (2014): Angular displacement and velocity sensors based on electric-LC (ELC) loaded microstrip lines. *IEEE Sensors Journal*, to be published.

**Naqui, J; Damm, C; Wiens, A; Jakoby, R; Su, L; Martín, F.** (2014): Transmission lines loaded with pairs of magnetically coupled stepped impedance resonators (SIRs): modeling and application to microwave sensors. *IEEE MTT-S Int. Microwave Symp.*, Tampa, USA, accepted.

**Pendry, J. B; Holden, A. J.; Robbins, D. J.; Stewart, W. J.** (1998): Low frequency plasmons in thin-wire structures. *J. Phys. Condens. Matter*, vol. 10, pp. 4785-4810.

**Pendry, J. B.; Holden, A. J.; Robbins, D. J.; Stewart, W. J.** (1999): Magnetism from conductors and enhanced nonlinear phenomena. *IEEE Trans. Microw. Theory Techn.,* vol. 47, pp. 2075-2084.

**Preradovic, S; Chandra-Karmakar, N.** (2010): Chipless RFID: bar code of the future. *IEEE Microw. Mag.*, vol. 11, pp. 87-98.

**Schurig, D.; Mock, J. J.; Smith, D. R.** (2006): Electric-field-coupled resonators for negative permittivity metamaterials. *Appl. Phys. Lett.*, vol. 88, paper 041109.

**Smith, D. R.; Padilla, W. J.; Vier, D. C.; Nemat-Nasser, S. C.; Schultz, S.**

(2000): Composite medium with simultaneously negative permeability and permittivity. *Phys. Rev. Lett.*, vol. 84, pp. 4184-4187.

**Tsai, C.-H.; Wu, T.-L.** (2010): A broadband and miniaturized common-mode filter for gigahertz differential signals based on negative-permittivity metamaterials. *IEEE Trans. Microw. Theory Techn.*, vol. 58, no. 1, pp. 195-202.

**Tseng, B. C.; Wu, L. K.** (2004): Design of miniaturized common-mode filter by multilayer low-temperature co-fired ceramic. *IEEE Trans. Electromagn. Compat.*, vol. 46, no. 4, pp. 571-579.

**Wu, S.-J.; Tsai, C.-H.; Wu, T.-L.; Itoh, T.** (2009): A novel wideband common-mode suppression filter for gigahertz differential signals using coupled patterned ground structure. *IEEE Trans. Microw. Theory Techn.*, vol. 57, no. 4, pp. 848-855.